AGU PUBLICATIONS

Tectonics

RESEARCH ARTICLE
10.1002/2013TC003512

Key Points:
- Slip rates on the Lone Mountain fault have accelerated since late Pleistocene
- Accelerating slip rates may reconcile long- and short-term rate discrepancies
- Several possible mechanisms for accelerating slip rates

Supporting Information:
- Readme
- Figure S1
- Figure S2
- Figure S3
- Figure S4
- Figure S5
- Figure S6
- Figure S7
- Figure S8
- Figure S9
- Figure S10
- Figure S11
- Figure S12
- Figure S13
- Figure S14
- Figure S15
- Table S1

Correspondence to:
Z. M. Lifton,
zlifton@gmail.com

Citation:
Lifton, Z. M., K. L. Frankel, and A. V. Newman (2015), Latest Pleistocene and Holocene slip rates on the Lone Mountain fault: Evidence for accelerating slip in the Silver Peak-Lone Mountain extensional complex, *Tectonics*, *34*, 449–463, doi:10.1002/2013TC003512.

Received 18 DEC 2013
Accepted 10 FEB 2015
Accepted article online 14 FEB 2015
Published online 16 MAR 2015

Latest Pleistocene and Holocene slip rates on the Lone Mountain fault: Evidence for accelerating slip in the Silver Peak-Lone Mountain extensional complex

Zachery M. Lifton[1], Kurt L. Frankel[1], and Andrew V. Newman[1]

[1]School of Earth and Atmospheric Sciences, Georgia Institute of Technology, Atlanta, Georgia, USA

Abstract Determining the constancy of fault slip rates over time is critical in characterizing strain distribution across plate boundaries such as the Pacific-North American plate boundary in the western U.S. We present results from the Lone Mountain fault, a normal fault within the southern Walker Lane, that suggest slip rates there may have increased approximately twofold since the late Pleistocene. We combine detailed field surficial mapping, topographic surveying, and ^{10}Be cosmogenic nuclide exposure ages to calculate new late Pleistocene and Holocene slip rates on the Lone Mountain fault. Alluvial fans with ages of 14.6 ± 1.4 ka and 8.0 ± 0.9 ka are vertically offset 10.2 ± 0.6 m and 4.7 ± 0.6 m, respectively, yielding vertical slip rates of 0.7 ± 0.1 mm/yr and 0.6 ± 0.1 mm/yr. These slip rates are faster than the rates of 0.1 to 0.4 mm/yr from earlier in the Pleistocene, defining a pattern of accelerating slip on the Lone Mountain fault over a timescale of 10^4 years. The possibility of accelerating slip rates in parts of the Walker Lane partially reconciles the observed discrepancy between long- and short-term slip rates in this region and elucidates the distribution of strain across an evolving plate boundary.

1. Introduction

The Pacific-North American plate boundary accommodates ~51 mm/yr of relative motion across a wide zone along the southwestern margin of North America [*DeMets et al.*, 2010]. Approximately 20% of that motion is accommodated in the Walker Lane, a diffuse, ~50–100 km wide right-lateral shear zone (Figure 1) [*Dixon et al.*, 2000; *Wesnousky*, 2005; *Lifton et al.*, 2013]. A distinct discrepancy has been observed between short- and long-term slip rates across the southern Walker Lane. The short-term right-lateral slip rate across the shear zone at about 37.5°N (latitude of this study), modeled from GPS measurements, is 10.6 ± 0.5 mm/yr [*Lifton et al.*, 2013]. However, the sum of geologic slip rates, estimated from paleoseismic and geomorphologic studies of individual faults, is only ~6 mm/yr [*Kirby et al.*, 2006; *Ganev et al.*, 2010; *Frankel et al.*, 2011; *Reheis and Sawyer*, 1997; *Foy et al.*, 2012; *Hoeft and Frankel*, 2010]. North of the Mina deflection in the central and northern Walker Lane, *Wesnousky et al.* [2012] proposed that the observed discrepancy between long- and short-term slip rates is reconciled when en echelon extensional basin opening and vertical axis rotation are taken into account. Reconciling this discrepancy in the southern Walker Lane is critical for understanding plate boundary strain distribution.

Strain is transferred through the southern Walker Lane primarily through north-northwest striking right-lateral strike-slip faults, such as the Death Valley fault, Fish Lake Valley fault, Owens Valley fault, and White Mountains fault zone. Strain is transferred between these subparallel strike-slip faults by northeast striking extensional step over faults [e.g., *Oldow et al.*, 1994; *Dixon et al.*, 1995; *Reheis and Dixon*, 1996], such as Tin Mountain fault, Deep Springs fault [*Lee et al.*, 2001], and Queen Valley fault [*Lee et al.*, 2009b] (Figure 1).

Oldow et al. [1994, 2009] proposed that the Silver Peak-Lone Mountain (SPLM) extensional complex is one such extensional step over, transferring strain from the Fish Lake Valley Fault to the Benton Springs and Petrified Springs fault zones in the central Walker Lane to the northeast (Figure 1). Similarly, *Frankel et al.* [2007a] and *Frankel et al.* [2011] proposed that the northward decrease in slip rate on the Fish Lake Valley fault is the result of distributed strain across the SPLM. The SPLM consists of a series of northeast trending normal faults, including Emigrant Peak, Clayton Valley, and Lone Mountain faults, which all have evidence of Quaternary displacements (Figure 1).

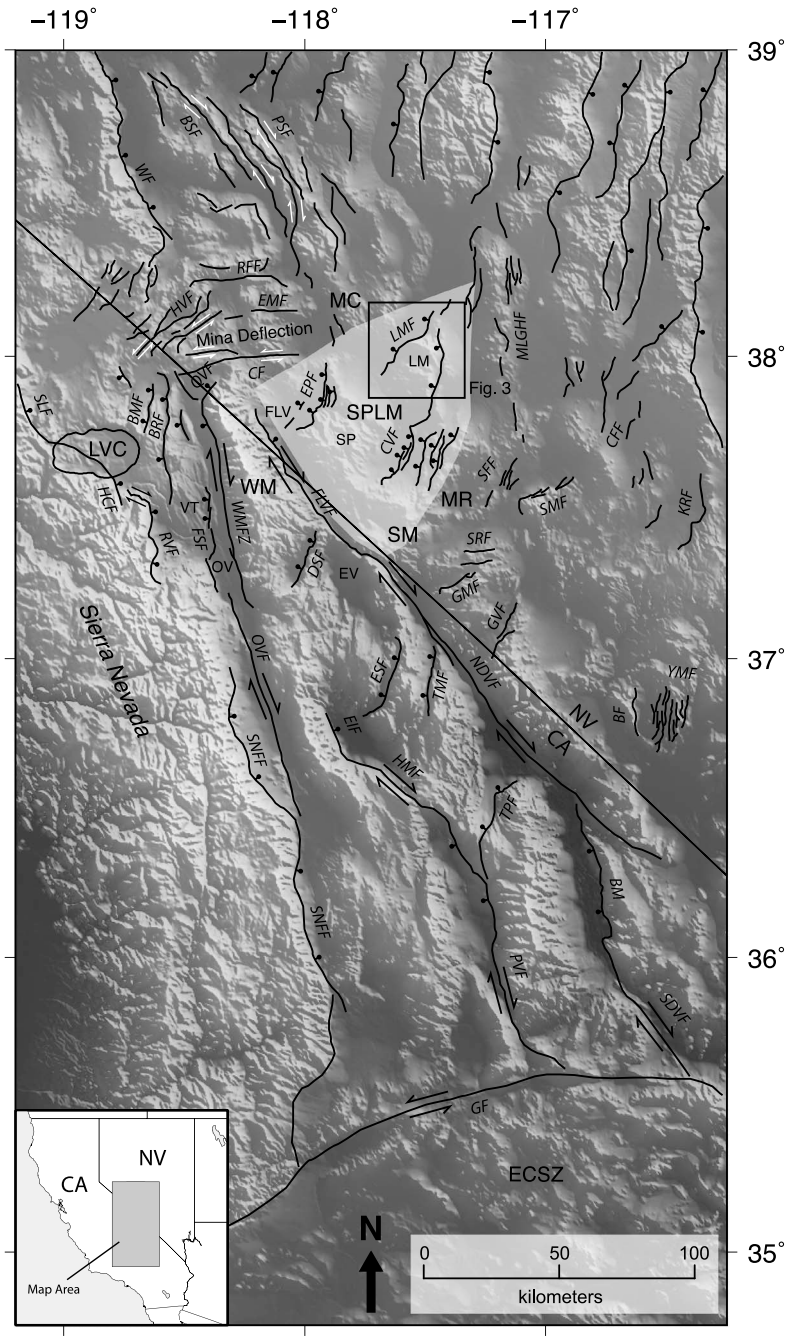

Figure 1. Shaded relief map of the southern Walker Lane showing simplified major Quaternary faults [*Ryan et al.*, 2009; *GMRT*, 2013; *U.S. Geological Survey et al.*, 2006]. Light gray shaded region is the Silver Peak-Lone Mountain extensional complex. BF, Bare Mountain fault; BMF, Black Mountain fault; BM, Black Mountain fault (Death Valley); BRF, Benton Range fault; BSF, Benton Springs fault; CF, Coaldale fault; CFF, Cactus Flat faults; CVF, Clayton Valley fault; DSF, Deep Springs fault; ECSZ, Eastern California Shear Zone; EIF, Eastern Inyo fault; EMF, Excelsior Mountains fault; EPF, Emigrant Peak fault; ESF, Eureka-Saline fault; EV, Eureka Valley; FSF, Fish Slough fault; FLV, Fish Lake Valley; FLVF, Fish Lake Valley fault; GF, Garlock fault; GMF, Gold Mountain fault; GVF, Grapevine Mountain fault; HCF, Hilton Creek fault; HMF, Hunter Mountain fault; HVF, Huntoon Valley fault; KRF, Kawich Range fault; LM, Lone Mountain; LMF, Lone Mountain fault; LVC, Long Valley Caldera; MC, Monte Cristo Range; MLGHF, Mud Lake-Goldfield Hills fault; MR, Montezuma Range; NDVF, Northern Death Valley fault; OV, Owens Valley; OVF, Owens Valley fault; PSF, Petrified Springs fault; PVF, Panamint Valley fault; QVF, Queen Valley fault; RFF, Rattlesnake Flat fault; RVF, Round Valley fault; SDVF, Southern Death Valley fault; SLF, Silver Lake fault; SFF, Stonewall Flat fault; SM, Sylvania Mountains; SMF, Stonewall Mountain fault; SNFF, Sierra Nevada frontal fault; SP, Silver Peak Range; SPLM, Silver Peak-Lone Mountain extensional complex; SRF, Slate Ridge fault; TMF, Tin Mountain fault; TPF, Towne Pass fault; VT, Volcanic Tableland; WM, White Mountains; WMFZ, White Mountains fault zone; WF, Wassuk Range fault; and YMF, Yucca Mountain fault.

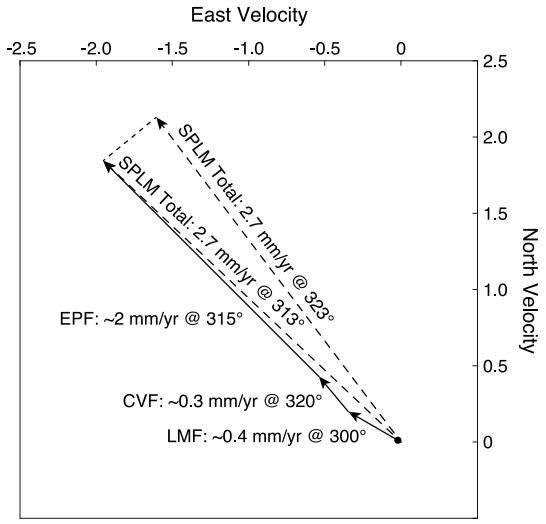

Figure 2. Velocity vector diagram of geologic slip rates previously reported in the SPLM. The sum of velocities is reprojected to the direction of local plate boundary motion of 323° [*Dixon et al.*, 2000]. EPF, Emigrant Peak fault [*Reheis and Sawyer*, 1997]; CVF, Clayton Valley fault [*Foy et al.*, 2012]; and LMF, Lone Mountain fault [*Hoeft and Frankel*, 2010].

Using geologic and geomorphologic mapping and terrestrial cosmogenic nuclide (TCN) geochronology, *Hoeft and Frankel* [2010] suggested that extension rates on the Lone Mountain fault may have increased between 92 ka and 17 ka, from 0.1 mm/yr to 0.4 mm/yr. We test the hypothesis that slip rates on the Lone Mountain fault continued to increase from latest Pleistocene through the Holocene, and that the SPLM may be accommodating a larger portion of plate boundary deformation than previously known. We estimate vertical and horizontal slip rates by combining measurements of displacement with ^{10}Be TCN exposure ages from boulders on two offset alluvial fan surfaces.

1.1. Tectonic and Geologic Setting

The SPLM is bounded on the west by the Fish Lake Valley fault, on the south by the Sylvania Mountains and the Montezuma Range, and on the north by the Candelaria Hills and Monte Cristo Range (Figure 1). The eastern boundary is not well defined but lies east of Lone Mountain [*Oldow et al.*, 2008].

Extension in the SPLM initiated at ~12–8 Ma as a northwest dipping detachment and was active until ~3 Ma, when 20°–30° of clockwise vertical axis rotation created long-wavelength (20–30 km), high-amplitude (1–2 km) folds in the detachment, which eventually locked motion on the fault. The detachment is now exposed in the Silver Peak Range and at Lone Mountain, where it separates deformed amphibolite facies rocks in the lower plate from Cenozoic volcanics and Mesozoic intrusive rocks in the upper plate. As the SPLM detachment shut down, the Mina deflection became the active slip transfer system connecting the southern and central Walker Lane [*Oldow et al.,* 2008].

Prominent Quaternary fault scarps are expressed along the Emigrant Peak, Clayton Valley, and Lone Mountain faults, which together accommodate much of the deformation across the SPLM (Figures 1 and 3). *Reheis and Sawyer* [1997] reported a minimum of 125 m of vertical offset since 760 ka, 30–66 m of vertical offset since 50–75 ka, and $22+4/-2$ m of vertical offset since 6.5 ± 1.5 ka on the Emigrant Peak fault. From these offset and age assignments, *Reheis and Sawyer* [1997] estimated vertical slip rates of 0.2, 0.4–1.2, and ~3 mm/yr, respectively. In an effort to quantify the uncertainties in the *Reheis and Sawyer* [1997] estimates, we used *Zechar and Frankel*'s [2009] probabilistic methods to calculate vertical slip rates of ~0.2 mm/yr, 0.8 ± 0.2 mm/yr, and $3.4+1.2/-0.8$ mm/yr, respectively, from their data. To place the role of the Emigrant Peak fault in the context of regional extension, the vertical slip rates were converted to horizontal extension rates based on the 45° to 70° dip of the fault reported by *Reheis and Sawyer* [1997] and a preferred dip of 60°. The resulting horizontal extension rates in the 315° direction based on *Reheis and Sawyer*'s [1997] preferred dip are ~0.1 mm/yr since 760 ka (<0.1 mm/yr at 70° dip, ~0.2 mm/yr at 45° dip), ~0.5 mm/yr since 50–75 ka (0.3 mm/yr at 70° dip, 0.8 mm/yr at 45° dip), and ~2 mm/yr since 6.5 ± 1.5 ka, (1.2 mm/yr at 70° dip, 3.4 mm/yr at 45° dip), defining a pattern of increasing slip rate. *Foy et al.* [2012] report a horizontal extension rate on the Clayton Valley since ~17 ka to be 0.1 to 0.3 mm/yr toward 320°. *Hoeft and Frankel* [2010] report horizontal extension rates across the Lone Mountain fault to be 0.1 to 0.4 mm/yr toward 300° since ~17 ka. We project these horizontal rates to the local plate motion direction of 323° [*Dixon et al.*, 2000] in order to understand their contribution to the overall plate boundary strain field. The sum of previously reported geologic extension rates since the late Pleistocene directed toward 323° across the SPLM is ~2.7 mm/yr (Figure 2).

Comparisons of geologic and geodetic right-lateral slip rates have also been made in the central and northern Walker Lane, north of the Mina Deflection. For example, *Wesnousky et al.* [2012] proposed that the sum of long-term geologic slip rates and short-term geodetic rates across the northern Walker Lane is approximately equal if the geologic slip rates take into account contributions from basin opening and

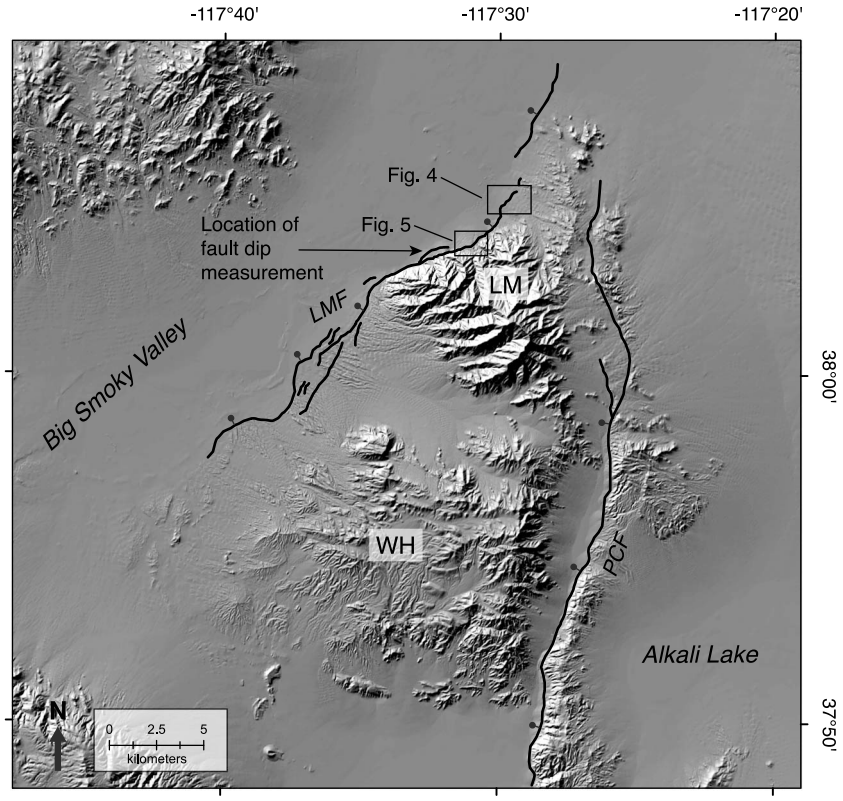

Figure 3. Shaded relief map of Lone Mountain (LM) and Weepah Hills (WH) showing the Lone Mountain fault (LMF) and locations of detailed alluvial fan maps (Figures 4 and 5). PCF, Paymaster Canyon fault.

vertical axis rotation. This suggests that distributed deformation may play an important role in strain accommodation in the Walker Lane.

The Lone Mountain fault is a northeast striking down-to-the-northwest normal fault that bounds the northwest side of Lone Mountain and the Weepah Hills (Figure 3). Along its southwestern portion, the Lone Mountain fault cuts the low hills and broad alluvial piedmont of the Weepah Hills. The fault is expressed as scarps that progressively increase in height with age, ranging from ~1 m to ~17 m in height. Along its northeastern portion, the fault delineates the bedrock-alluvium interface, offsetting young, steep alluvial fans and in some cases offsetting bedrock. Farther to the northeast, the Lone Mountain fault diverges from the range front, offsetting alluvial fans and its surface expression diminishes. *Hoeft and Frankel* [2010], *Hoeft* [2010], and *Hoeft and Frankel* [2012] mapped the southwestern part of Lone Mountain fault through the alluvial piedmont of the Weepah Hills and Lone Mountain range front, and estimated cosmogenic nuclide exposure ages for three alluvial fans displaced by the fault. We expand upon the work of *Hoeft and Frankel* [2010] by mapping part of the northeast portion of the Lone Mountain fault and estimating cosmogenic nuclide exposure ages on two alluvial fans displaced by the fault. This work not only expands the spatial extent of mapping of the Lone Mountain fault but also extends the temporal range of fault slip rate estimates.

2. Alluvial Fan Mapping

We mapped alluvial fan units and fault scarps at two sites along the Lone Mountain fault (Figures 3–5). Mapping was conducted on U.S. Department of Agriculture 1 m resolution color orthorectified aerial photograph basemaps at scales of 1:5000 and 1:8000. Alluvial fan units were organized into the chronostratigraphic framework of *Bull* [1991], in which fan units are differentiated by criteria such as elevation above the active channel, extent of pavement and varnish development, bar and swale morphology, and degree of surface dissection. Below we describe the individual displaced alluvial fan units we mapped.

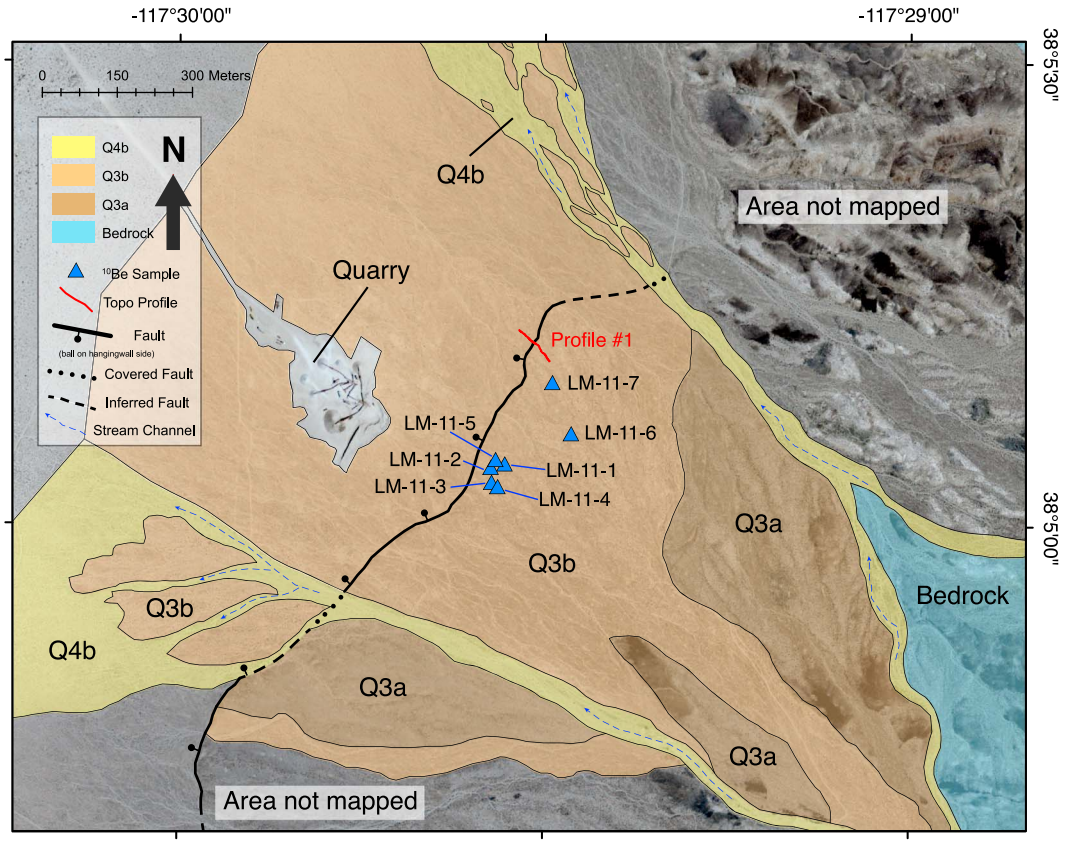

Figure 4. Surficial geologic map showing the location of Q3b alluvial fan offset by the Lone Mountain fault and sample locations (blue triangles). Red line is location of topographic profile across (Profile #1) the fault scarp (Figure 6a). Blue dashed lines with arrows indicate streamflow direction.

2.1. Descriptions of Alluvial Fan Units

2.1.1. Q3a Alluvial Fan

The Q3a alluvial fan is preserved in only a few locations in our mapping area, and we were not able to quantify its displacement. This fan surface has a subdued bar and swale morphology with vertical relief less than 1 m. The surface is relatively planar and is not deeply incised by stream channels. Desert pavement and desert varnish are moderately developed, giving the surface a darker color than the Q3b fan surface. The Q3a fan surface elevation is ≥3 m above the active channel.

2.1.2. Q3b Alluvial Fan

The Q3b alluvial fan has subdued bar and swale morphology with vertical relief of less than 1 m. The surface has moderately developed pavement, with swale areas composed of a loosely interlocking pavement of gravel- and cobble-sized clasts with some sand and minor silt, and bar areas composed of cobble-sized clasts and rare boulder-sized clasts. The lithology of the sediment is primarily granitic intrusive rock, which weathers to grus. Some clasts are moderately weathered. Boulders and cobbles have moderately developed varnish and rubification, and clasts on this surface are generally lightly weathered. The Q3b has a ~10 cm thick Av horizon with some vesicles. The elevation of the Q3b surface is ~2 m above the active channel.

2.1.3. Q3c Alluvial Fan

The Q3c alluvial fan has prominent bouldery bar and swale morphology that is beginning to diffuse. The bar and swale morphology has a wavelength of ~3 m and amplitude of ~1–2 m. Desert pavement is poorly developed, and varnish and rubification is absent to moderately developed on boulders and cobbles. Sediment is primarily derived from granitic intrusive rock. Some clasts are lightly to moderately weathered. Boulders are more pervasive across the Q3c fan than the Q3b surface, which we attribute to its proximity to the source area. This fan has a poorly developed, nonvesicular Av horizon that is ~5 cm thick. Some

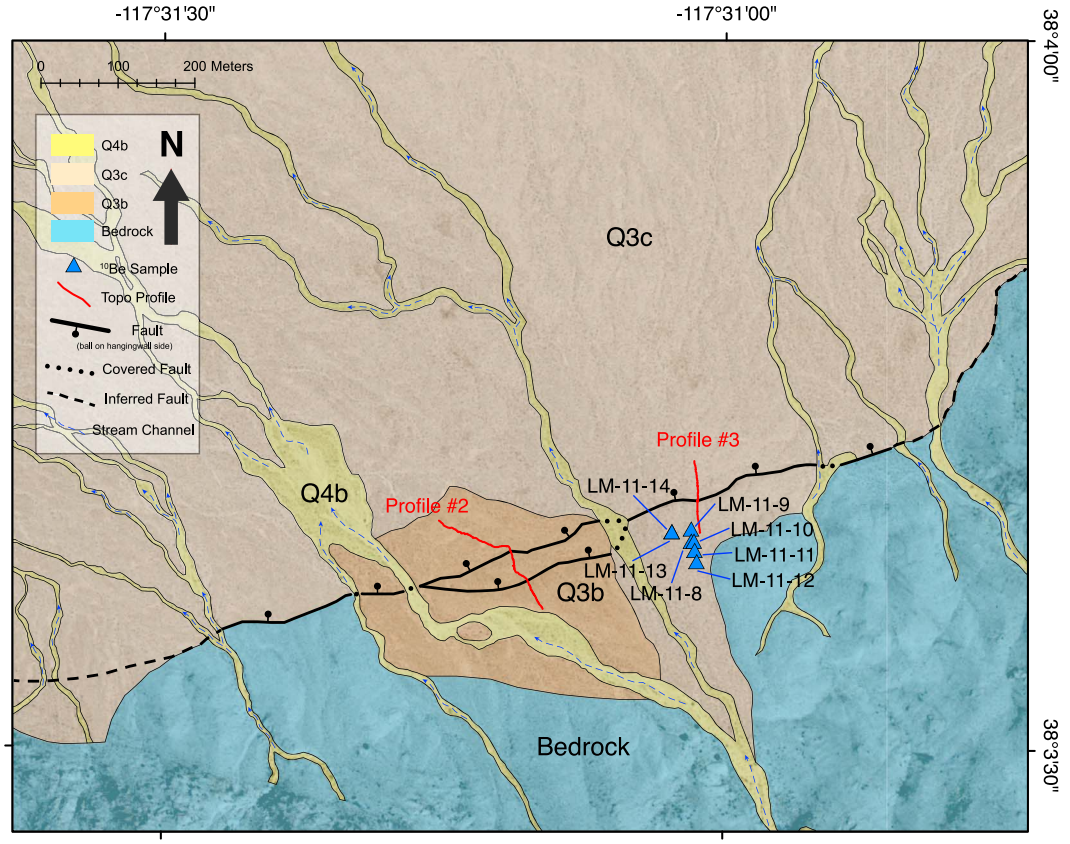

Figure 5. Surficial geologic map showing the location of Q3b and Q3c alluvial fans offset by the Lone Mountain fault and sample locations (blue triangles). Red lines are locations of topographic profiles (Profiles #2 and #3) across the fault scarp (Figures 6b and 6c). Blue dashed lines with arrows indicate streamflow direction.

portions of the fan have a well-developed biotic crust that appears darker than the rest of the fan surface. The elevation of the Q3c surface is ~1–2 m above the active channel.

2.1.4. Q4b Alluvial Fan

The Q4b alluvial fan unit is associated with the active stream channel network. It is composed of boulders, cobbles, and gravel within channels incised into surrounding fans. Bar and swale morphology is prominent and well defined. Desert pavement and varnish are absent, and clasts are generally fresh and unweathered. The surface of the Q4b deposit is lighter in color than older deposits.

3. Alluvial Fan Displacement

We measured topographic profiles across fault scarps using a Trimble GeoXH handheld Global Positioning System (GPS) unit. Differential corrections were made in postprocessing with data from nearby Continuously Operating Reference Station sites. Profiles are orthogonal to the fault, where they cross the scarp and follow the fan surfaces along the apex-to-toe fall line. All of the profiles used in this study were measured where the original fan surface is preserved in both the footwall and hanging wall. We did not observe any evidence of strike-slip motion on the fault. Topographic profiles across the fault scarp are presented in Figure 6. We selected profile points along the footwall and hanging wall surfaces and calculated best fit linear regressions to those points. We projected the linear regressions to the scarp and measured the vertical offset between the surfaces at the center of the scarp. We measured vertical offset of the Q3b fan surface in two locations (Figures 4–6). The location at which we sampled the Q3b surface is vertically offset 2.4 ± 0.6 m (Figures 4 and 6a). However, the combined vertical offset was observed to be 10.2 ± 0.6 m across two closely spaced faults offsetting a correlative Q3b fan nearby (Figures 5 and 6b). We interpreted the two Q3b surfaces to be correlative based on degree of desert pavement and desert varnish development, bar and swale morphology, and relative

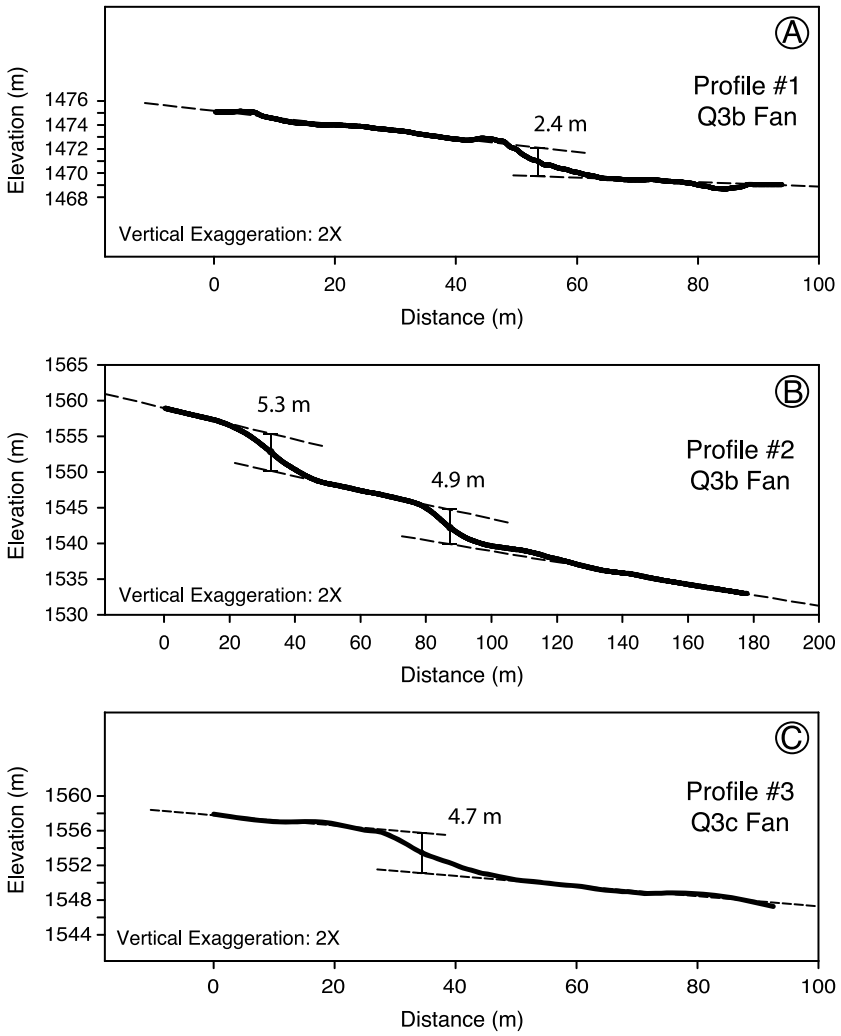

Figure 6. Topographic profiles across the Lone Mountain fault scarp in the (a) Q3b alluvial fan, (b) Q3b alluvial fan (double scarp), and (c) Q3c alluvial fan.

fan surface height. Therefore, we used the larger displacement across the surface to calculate the extension rate. While the footwall and hanging wall surfaces were visibly indistinguishable in field observations, we consider the vertical offset measurements to be minima, allowing for possible aggradation of the hanging wall surface after displacement. The Q3c surface is vertically offset 4.7 ± 0.6 m (Figures 5 and 6c). Uncertainties in vertical displacement measurements are estimated from formal errors reported by the differentially corrected GPS positions in the topographic profiles and from the uncertainty in the linear regressions fits to the measured surfaces. The differential GPS positions reported a vertical uncertainty of ~ ±0.3 m, while the maximum uncertainty of the linear regressions is ~±0.2 m or less. Combining these uncertainties and propagating them through the measurement yields an uncertainty estimate of ±0.6 m. This uncertainty is likely an overestimate since the GPS vertical errors are highly correlated in time and position, suggesting that the true GPS error across an individual profile is smaller.

The relatively small displacement of the Q3c fan (4.7 ± 0.6 m) raises the possibility that it records only a single surface rupturing slip event. In such a case, our reported slip rate may be biased either positively or negatively depending on the temporal sampling window relative to the earthquake cycle. Accurate calculation of geologic slip rates necessitates capturing multiple slip events across multiple seismic cycles to account for variances in earthquake episodicity and slip magnitude over cycles. To illustrate with an extreme example, if a fault ruptured 5 m 10 years ago, the apparent slip rate would be 500 mm/yr; however, if the earthquake

Table 1. Offset, Alluvial Fan Exposure Ages, and Slip Rates Along Lone Mountain Fault

Alluvial Fan Deposit	Vertical Offset (m)	Extension Direction (deg)	Age (ka)	Vertical Slip Rate (mm/yr)	Horizontal Slip Rate (mm/yr)			Slip Rate Toward 323° (mm/yr)[b]
					Dip = 30°	Dip = 60°	Dip = 40°[a]	
Q3b	10.2 ± 0.6	340	14.6 ± 1.4	0.7 ± 0.1	1.2 ± 0.2	0.4 ± 0.1	0.8 ± 0.1	0.8 ± 0.1
Q3c	4.7 ± 0.6	340	8.0 ± 0.9	0.6 ± 0.1	1.0 ± 0.2	0.3 ± 0.1	0.7 ± 0.1	0.7 ± 0.1
Q3c[c]				1.2 to 0.3	2.1 to 0.6	0.7 to 0.2	1.4 to 0.4	1.4 to 0.4

[a]Preferred fault dip based on field observation.
[b]Horizontal slip rate projected parallel to Pacific-North America plate motion [*Dixon et al.*, 2000].
[c]Q3c surface possible rates assuming maximum and minimum values for a single offset event.

cycle duration is actually 5000 years, then the true slip rate is 1 mm/yr. If the recurrence interval and slip on a fault were perfectly regular, then observing a single, complete earthquake cycle would be sufficient to calculate a valid slip rate.

Based on historical data from normal faults of similar length in the Basin and Range and empirical scaling relationships, we believe the Q3c scarp may represent two or more rupture events. The 1983 M_s 7.3 Borah Peak earthquake produced a 34 km long surface rupture, with a maximum vertical displacement of 2.7 m [*Crone and Machette*, 1984]. There is evidence for larger local maximum displacements, for example, the largest historic vertical offset in the Basin and Range occurred during the 1915 M_s 7.6 Pleasant Valley earthquake, which produced a 60 km long surface rupture with a maximum vertical displacement of 5.8 m [*dePolo et al.*, 1991]. Additionally, based on trenching and fault scarp profiling, *Koehler and Wesnousky* [2011] determined that the maximum single event displacement along the ~32 km long Simpson Park Mountains fault was 4.2 m. However, these examples appear to be exceptional, given that the scaling relationship developed for normal faults by *Wells and Coppersmith* [1994] predicts a maximum displacement of $<$2 m for a 30 km long fault rupture. If the typical rupture is 2–3 m along such a segment, then it is more likely that the 4.7 ± 0.6 m of vertical displacement of the Q3c fan represents at least two ruptures of the Lone Mountain fault. While this would yield a valid slip rate, it could still be biased depending upon the uniformity of the earthquake cycle duration.

If the Q3c surface was only offset in a single, anomalously large event, then the true earthquake recurrence is not known. At the shortest end, the Q3c surface was formed immediately after a prior event, and another is imminently due. In such a hypothetical scenario, the true recurrence is about one half the Q3c age, bringing the vertical slip rate to a maximum of 1.2 mm/yr. At the longest reasonable end, the Q3c surface captured a single event on a fault with a longer recurrence. Since the adjacent faults that offset the older Q3b surface require multiple ruptures (having at least 10 m of cumulative slip across one profile) since 14.6 ka, it is possible that the maximum regular recurrence interval is just under that age. This would yield an extreme minimum long-term slip rate of 0.3 mm/yr, comparable to earlier estimates. Because 1.2 and 0.3 mm/yr are extreme cases, assuming a single large slip event that we consider less likely, we exclude them from further discussion, but include them in Table 1.

4. Cosmogenic Nuclide Exposure Ages

We estimated the age of displaced fan surfaces by ^{10}Be TCN exposure dating of boulders deposited on the fan surfaces. Boulders embedded in the alluvial fan surface are exposed to cosmic rays, which interact with Si and O atoms in minerals and produce ^{10}Be nuclides. The concentration of ^{10}Be nuclides is a function of exposure time, rock density, radioactive decay, erosion, and inheritance from previous exposure [*Lal*, 1991; *Gosse and Phillips*, 2001].

We sampled seven boulders from the Q3b surface and seven boulders from the Q3c surface (see Figures 4 and 5 and Table S1 in the supporting information for locations). Samples were collected from the upper $\leq$5 cm of the top of each boulder. We sampled boulders that were in place and exposed at the surface since deposition. In particular, we chose boulders that were located on flat surfaces, away from the fan surface edges where diffusive processes can move sediment. We also chose boulders that were not weathered, that had desert varnish on the top of the boulder only, and that did not appear to be exhumed.

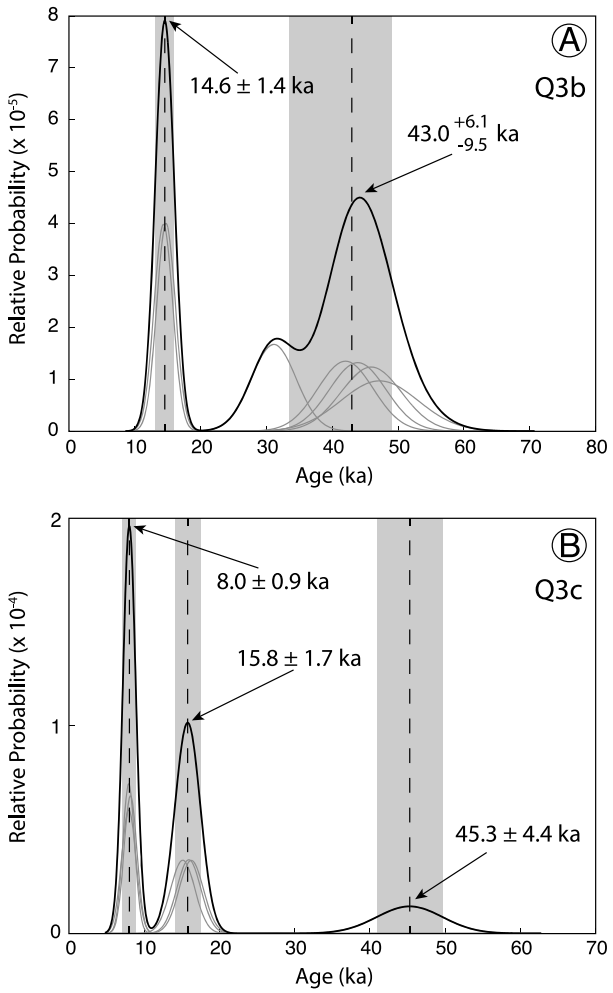

Figure 7. Probability density function (PDF) of ^{10}Be exposure ages from (a) seven boulder samples on the Q3b fan surface and (b) seven boulder samples on the Q3c fan surface. Gray curves are individual PDFs for each boulder, and black curve is the combined PDF for all ages. Vertical gray bands represent the 1σ uncertainty interval for the weighted mean ages of each peak. Note the consistency of age clusters between the two fans.

In cases where boulders were weathered or spalled, we sampled only the intact, unweathered areas of the boulder. See supporting information for photographs of each sample.

Since the full history of individual boulders is not known, it is possible that the ^{10}Be age of a given boulder may appear older or younger than the true exposure age. For example, some boulders contain "inherited" ^{10}Be nuclides from surface exposure prior to deposition in the current alluvial fan, which yields artificially old ^{10}Be ages. Conversely, exhumation of buried boulders and weathering (e.g., spalling) can yield apparent boulder ages that are younger than the true exposure age of the fan. To avoid artificially young boulder ages of the latter case, we only sampled boulder surfaces that were not weathered and that had well-developed desert varnish. Inheritance can be quantified by sampling at intervals below the surface within a soil pit to create a depth profile of ^{10}Be concentration [e.g., *Anderson et al.*, 1996]; however, the very large grain size of the alluvial fan sediment made it impractical to dig soil pits and precluded our use of depth profiles. Furthermore, the lack of large exposures of fine-grained sediments in the alluvial fans also precluded the use of optically stimulated luminescence dating. In order to address potential inheritance in ^{10}Be concentrations of surface boulders, we assume that the youngest ages (i.e., the lowest ^{10}Be concentrations and shortest surface exposure durations) within a population of samples are the best representation of the age of the current alluvial fan deposit [*Hoeft and Frankel*, 2010; *Owen et al.*, 2002, 2005]. While older samples (i.e., longer surface exposure duration and higher ^{10}Be concentrations) may exist within the population due to inheritance, surface boulders cannot be younger than the alluvial fan deposit.

Each surface sample was prepared and measured separately following the methods of *Kohl and Nishiizumi* [1992]. Samples were crushed, pulverized, and sieved to isolate the 250–500 μm size fraction. Quartz was isolated and purified with a series of HF leaches in heated ultrasonic tanks. After dissolution, Be was extracted from the quartz by ion exchange chromatography, then precipitated as $Be(OH)_2$ and oxidized to BeO. The BeO was mixed with niobium powder and packed in a target. The ^{10}Be/^{9}Be ratio of each sample was measured by accelerator mass spectrometry at the Purdue Rare Isotope Measurement Laboratory. Isotopic ratios were normalized to standard 07KNSTD3110 with a value of 2.85×10^{-12} [*Nishiizumi et al.*, 2007]. Results are reported in Table S1 in the supporting information.

Exposure ages for each sample are modeled using the CRONUS-Earth age calculator [*Balco et al.*, 2008], using a time-invariant sea level, high-latitude ^{10}Be production rate of 4.76 atoms g^{-1} a^{-1}, scaled for our locations

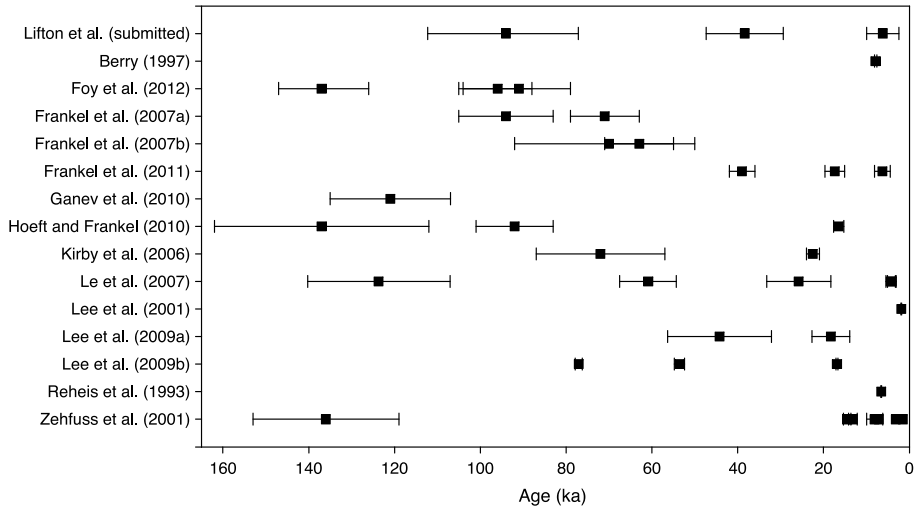

Figure 8. Compilation of published alluvial fan ages in the Walker Lane, eastern California shear zone, and Death Valley.

[*Lal*, 1991; *Stone,* 2000; *Nishiizumi et al.*, 2007]. Ages and their associated uncertainties are combined in a probability density function (PDF) to determine the weighted mean exposure age and 1σ uncertainty for each fan.

The exposure ages of individual boulders fall into several distinct clusters (Figure 7). On the Q3b fan, two boulders are ~15 ka, one boulder is ~31 ka, and the remaining four boulders are ~45 ka. On the Q3c fan, three boulders are ~8 ka, three boulders are ~16 ka, and one boulder is ~45 ka (Figure 7). The older exposure ages of some boulders reflect a more complex history of deposition and exposure in an older fan, remobilization and transport, and finally deposition and exposure in the current fan deposit. Because boulders can contain inherited ^{10}Be from previous exposure prior to deposition in their present locations, we assume that the youngest clusters of ages are the best representation of the exposure age of the current alluvial fans [e.g., *Hoeft and Frankel*, 2010; *Owen et al.*, 2002, 2005]. We calculated the weighted mean average of each cluster of ages (Figure 7). The ^{10}Be exposure age of the Q3b fan is 14.6 ± 1.4 ka, and the ^{10}Be exposure age of the Q3c fan is 8.0 ± 0.9 ka (Table 1). The Q3b fan age is the same, within uncertainty, as a nearby Q3b fan dated to 16.5 ± 1.2 ka by *Hoeft and Frankel* [2010]. Our fan exposure ages also agree with other fan ages reported across the Walker Lane, the eastern California shear zone, and the Death Valley region (Figure 8).

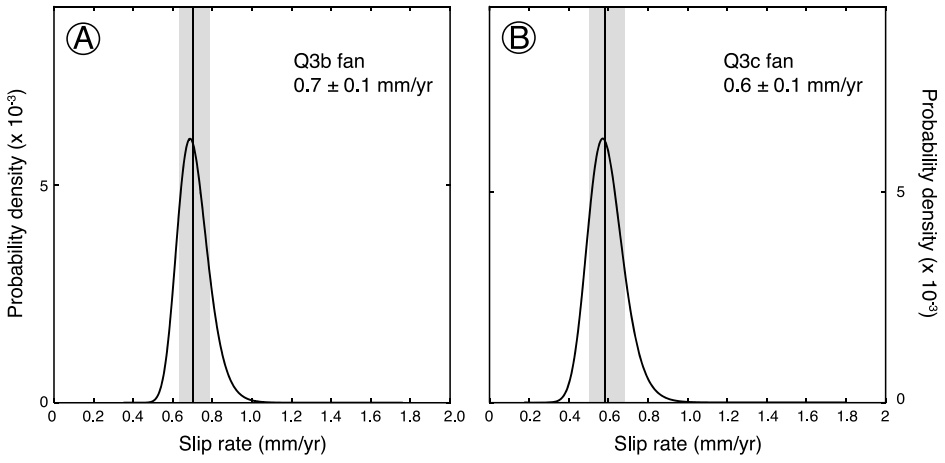

Figure 9. Vertical slip rate probability density functions for offset (a) Q3b and (b) Q3c alluvial fans. Vertical line represents the median age, and gray band represents the 1σ uncertainty interval.

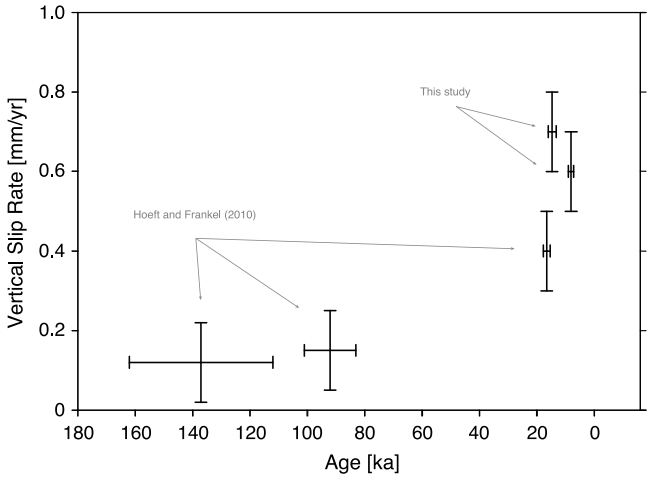

Figure 10. Compilation of vertical slip rates on the Lone Mountain fault over time. Horizontal error bars represent reported age uncertainties, and vertical error bars represent reported extension rate uncertainties.

5. Slip Rates

We used the methods of *Zechar and Frankel* [2009] to calculate vertical slip rates. This probabilistic approach treats the displacement, age, and slip rate as probability density functions and propagates uncertainties of each measurement through the calculation. All slip rates are reported with 1σ uncertainties. The results of our slip rate calculations are shown in Figures 9 and 10 and in Table 1. For the Q3b fan, the vertical displacement of 10.2 ± 0.6 m and the exposure age of 14.6 ± 1.4 ka yield a vertical slip rate of 0.7 ± 0.1 mm/yr. For the Q3c fan, the vertical displacement of 4.7 ± 0.6 m and the exposure age of 8.0 ± 0.9 ka yield a vertical slip rate of 0.6 ± 0.1 mm/yr.

These rates are minima because the fan exposure ages we use represent the earliest possible time that the fan was displaced, allowing for the possibility that the fans were displaced more recently. Several other factors may affect the accuracy of our slip rates. Because inheritance is difficult to quantify in surface samples, the fan ages may appear older than the true age, which would also bias our results toward slower slip rates. While quantification of inheritance in our samples is not possible, the geomorphological characteristics of the fans suggest that this is minimal. Additionally, ages from this study are in close agreement with other exposure ages reported in the region (Figure 8), suggesting neither overestimation (from inheritance) nor underestimation (from weathering and spalling of boulders) are major concerns. Field photos of sample sites are included in the supporting information.

From the vertical slip rates, we calculate horizontal extension rates in order to place the Lone Mountain fault in a more meaningful tectonic context relative to geodetic observations of regional extension. We approximate horizontal extension rates by assuming a range of frequently observed fault dips from 30° to 60° [e.g., *Wernicke*, 1995; *Olive and Behn*, 2014, and references therein]. Our preferred fault dip is 40°, observed in this study as well as *Hoeft and Frankel* [2010] along a 3 m to 4 m high-channel exposure cut into an unconsolidated Q3b fan deposit orthogonal to the fault strike. The fault dipped uniformly at 40° from the surface to a depth of 3–4 m and formed a narrow zone of disturbed clasts oriented approximately parallel to the fault plane (see supporting information). The behavior of normal faults at depth is often debated, and it is not known if dip at the surface or in unconsolidated material is an accurate representation of dip at depth [e.g., *Wernicke*, 1981; *Wernicke and Axen*, 1988; *Jackson and McKenzie*, 1983]. Without subsurface data to constrain fault dip, our best estimate is based on direct observation, and we therefore prefer a fault dip of 40°. Geophysical data suggest that the Clayton Valley fault dips ~60° [*McGuire et al.*, 2011].

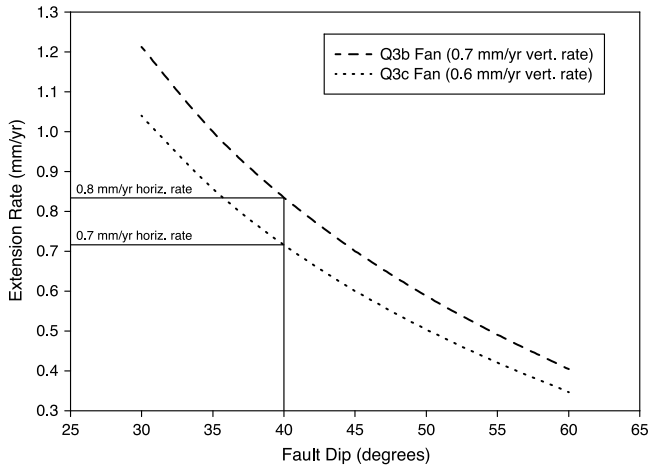

Figure 11. Graph of horizontal extension rate as a function of fault dip for the Q3b and Q3c fans. Our preferred fault dip is 40°, which yields horizontal slip rates of 0.8 ± 0.1 mm/yr and 0.7 ± 0.1 mm/yr for the Q3b and Q3c fans, respectively.

Reheis and Sawyer [1997] report the Emigrant Peak fault dips between 45° and 70°. Since most normal faults dip between 30° and 60°, we also present horizontal slip rates over this entire range of dips (Figure 11 and Table 1). For a fault dip of 30°, the Q3b horizontal slip rate is 1.2 ± 0.2 mm/yr and the Q3c horizontal slip rate is 1.0 ± 0.2 mm/yr. For a fault dip of 60°, the Q3b horizontal slip rate is 0.4 ± 0.1 mm/yr and the Q3c horizontal slip rate is 0.3 ± 0.1 mm/yr. For our preferred fault dip of 40°, the Q3b horizontal slip rate is 0.8 ± 0.1 mm/yr and the Q3c horizontal slip rate is 0.7 ± 0.1 mm/yr.

6. Discussion

Our results suggest that slip rates on the Lone Mountain fault increased from the late Pleistocene to the Holocene. The vertical slip rate since 14.6 ± 1.4 ka is 0.7 ± 0.1 mm/yr, and the vertical slip rate since 8.0 ± 0.9 ka is 0.6 ± 0.1 mm/yr. These rates are approximately twice as fast as the late Pleistocene slip rates on the Lone Mountain fault estimated by *Hoeft and Frankel* [2010] (0.1 to 0.4 mm/yr) but complement their conclusion that slip on the Lone Mountain fault is increasing (Figure 10). The accelerating slip rates that we observe on the Lone Mountain fault also agree with the pattern of increasing slip rates observed elsewhere in the SPLM, in particular on the Emigrant Peak fault [*Reheis and Sawyer*, 1997]. *Reheis and Sawyer* [1997] presented data that suggest the Emigrant Peak fault vertical slip rate was ~0.2 mm/yr since 760 ka, increased to 0.8 ± 0.2 mm/yr since 50–70 ka, and then increased further to 3.4 + 1.2/−0.8 mm/yr since 6.5 ± 1.5 ka.

The possibility of accelerating slip rates across the SPLM has implications for the evolution of the Walker Lane. In particular, it is important for understanding how the Walker Lane accommodates strain, and for comparing long- and short-term slip rates across the Walker Lane.

Variability in slip rates over different timescales of observation has been documented on a number of faults [e.g., *Dolan et al.*, 2007; *Friedrich et al.*, 2003; *Gold et al.*, 2013; *Kirby et al.*, 2006; *Reheis and Sawyer*, 1997; *Weldon et al.*, 2004], yet the cause is not well understood. Some studies suggest that maturation of fault systems [e.g., *Gourmelen et al.*, 2011] can yield variable slip rates by connecting smaller faults into faster through-going faults. In other cases, long distance fault interaction may account for local changes in fault slip rates [*Dolan et al.*, 2007; *Gold et al.*, 2013]. *Friedrich et al.* [2003] suggest that slip rate variability occurs at multiple timescales: variability due to changes in tectonic loading occurs at ~10 Myr timescales, clustered strain release due to fault system dynamics occurs at ~10 kyr timescales, and variability due to transient postseismic effects occurs at ~100 yr timescales. Clustering of earthquakes can yield variable slip rates depending on the time window of observation. The slip rate averaged over a period of closely spaced earthquakes will be faster than the slip rate averaged over a period of quiescence or over a period of many clusters. Identifying temporal clustering behavior requires a detailed chronology of ruptures, which we do not have for the Lone Mountain fault. Therefore, we can only speculate on the possibility of temporal clustering. The mechanism for accelerating slip rates on the Lone Mountain fault is not known, but it appears that Lone Mountain fault and Emigrant Peak fault have both accelerated on approximately the same timescale. This raises the possibility that the SPLM as a whole may be interacting with distant faults such as the Fish Lake Valley fault, as suggested by *Oldow et al.* [1994, 2009], *Frankel et al.* [2007a, 2011], and *Nagorsen-Rinke et al.* [2013].

Accelerating slip rates also have important implications for comparing long- and short-term slip rates across the Walker Lane. A discrepancy between long-term geologic slip rates and short-term geodetic slip rates has been observed across the Walker Lane at ~37°N latitude [*Bennett et al.*, 2003; *Kirby et al.*, 2006, 2008; *Frankel et al.*, 2007b, 2011; *Lifton et al.*, 2013]. The sum of published late Pleistocene slip rates from the Lone Mountain, Clayton Valley, Emigrant Peak, Fish Lake Valley, and White Mountains faults, projected toward the plate motion direction of 323°, across this part of the Walker Lane is ~6 mm/yr [*Kirby et al.*, 2006; *Ganev et al.*, 2010; *Frankel et al.*, 2011; *Reheis and Sawyer*, 1997; *Foy et al.*, 2012; *Hoeft and Frankel*, 2010]. However, dislocation models constrained by GPS data predict a regionally averaged short-term right-lateral displacement rate at ~37.5°N latitude of 10.6 ± 0.5 mm/yr [*Lifton et al.*, 2013]. The possibility that the SPLM is accommodating an increasing portion of shear zone-directed slip might help reconcile the discrepancy. Including our new Holocene extension rate of 0.7 ± 0.1 mm/yr slightly increases the sum of slip across the Walker Lane toward the plate motion direction of 323° to ~6.4 mm/yr. However, the sum is still significantly slower than the geodetic slip rate of 10.6 ± 0.5 mm/yr [*Lifton et al.*, 2013]. Recent studies [e.g., *Foy et al.*, 2012] suggest that a significant proportion of strain may be broadly distributed, and that extension rates in the SPLM might be significantly faster than documented. Furthermore, the Holocene extension rate on the Clayton Valley fault

is not known, but if it has experienced similar accelerated slip to the Emigrant Peak and Lone Mountain faults, then its more recent extension rate may also be faster.

Our results, in combination with observations of slip occurring both east of the Fish Lake Valley fault [e.g., *Reheis and Sawyer*, 1997; *Ganev et al.*, 2010; *Foy et al.*, 2012; *Hoeft and Frankel*, 2010] and west of the White Mountains fault [*Lienkaemper et al.*, 1987; *dePolo and Ramelli*, 1987; *Phillips and Majkowski*, 2011; *Nagorsen-Rinke et al.*, 2013], support the hypothesis of *Frankel et al.* [2011] that the Walker Lane south of the Mina deflection is accommodating strain in a broader region than previously suspected. In other words, rather than strain being restricted to a narrow zone of right-lateral slip on the White Mountains and Fish Lake Valley faults [*Reheis and Dixon*, 1996], slip is diffused across a broader region as it moves northward toward the Mina deflection.

7. Conclusions

We calculated vertical slip rates during the latest Pleistocene and Holocene on the Lone Mountain fault, which is a down-to-the-northwest normal fault in the Silver Peak-Lone Mountain extensional complex. Geologic mapping and topographic surveying yield vertical displacements of 10.2 ± 0.6 m and 4.7 ± 0.6 m for the Q3b and Q3c fans, respectively. The vertical slip rate since 14.6 ± 1.4 ka is 0.7 ± 0.1 mm/yr, and the vertical slip rate since 8.0 ± 0.9 ka is 0.6 ± 0.1 mm/yr. Horizontal slip rates could range from ~1.2 mm/yr to ~0.3 mm/yr for fault dips of 30° and 60°, respectively. For a preferred fault dip of 40° based on field observations, these vertical rates translate to horizontal slip rates of 0.8 ± 0.1 mm/yr and 0.7 ± 0.1 mm/yr, respectively. These new rates, in combination with previously published data [*Hoeft and Frankel*, 2010], suggest that slip on the Lone Mountain fault has increased during the late Pleistocene and Holocene (Figure 10). Incorporating our new rates with published slip rates in the region indicates that the total geologically determined slip rate in the 323° direction at this latitude is ~6.4 mm/yr. Thus, the possibility of accelerating slip rates within parts of the Walker Lane partially reconciles the observed discrepancy between long- and short-term slip rates in this region, especially if distributed deformation has resulted in undocumented displacement. The mechanism for fault slip acceleration on the Lone Mountain fault is unknown, but may be due to one of a number of mechanisms hypothesized to cause long-term variability in slip rates. These include long distance fault interactions, fault system reorganization, or clustering of strain release. Continued study of the Lone Mountain fault and the regional fault system within the Walker Lane could test these hypotheses.

Acknowledgments

This study was funded by NSF grant EAR-0948570, a University of California White Mountains Research Station minigrant, a GSA research grant, and a Sigma Xi grant-in-aid of research. We thank Chris Johnson for assistance with sample collection. Discussions with Jeff Lee and Tim Dixon helped clarify the paper. We thank the Editor, Associate Editor, Rich D. Koehler, and two anonymous reviewers for thoughtful reviews that significantly improved and clarified the manuscript.

References

Anderson, R. S., J. L. Repka, and G. S. Dick (1996), Explicit treatment of inheritance in dating depositional surfaces using in situ ^{10}Be and ^{26}Al, *Geology*, *24*, 47–51.

Balco, G., J. O. Stone, N. A. Lifton, and T. J. Dunai (2008), A complete and easily accessible means of calculating surface exposure ages or erosion rates from ^{10}Be and ^{26}Al measurements, *Quat. Geochronol.*, *3*, 174–195, doi:10.1016/j.quageo.2007.12.001.

Bennett, R., B. Wernicke, N. Niemi, A. Friedrich, and J. Davis, (2003), Contemporary strain rates in the northern Basin and Range province from GPS data, *Tectonics*, *22*(2), 1008, doi:10.1029/2001TC001355.

Berry, M. E. (1997), Geomorphic analysis of late Quaternary faulting on Hilton Creek, Round Valley and Coyote warp faults, east-central Sierra Nevada, California, USA, *Geomorphology*, *20*, 177–195.

Bull, W. B. (1991), *Geomorphic Responses to Climatic Change, New York, NY (United States)*, Oxford Univ. Press, New York.

Crone, A. J., and M. N. Machette (1984), Surface faulting accompanying the Borah Peak earthquake, central Idaho, *Geology*, *12*, 664, doi:10.1130/0091-7613(1984)12<664:SFATBP>2.0.CO;2.

DeMets, C., R. G. Gordon, and D. F. Argus (2010), Geologically current plate motions, *Geophys. J. Int.*, *181*, 1–80, doi:10.1111/j.1365-246X.2009.04491.x.

dePolo, C. M., and A. R. Ramelli (1987), Preliminary report on surface fractures along the White Mountains fault zone associated with the July 1986 Chalfant Valley earthquake sequence, *Bull. Seismol. Soc. Am.*, *77*, 290–296.

dePolo, C. M., D. G. Clark, D. B. Slemmons, and A. R. Ramelli (1991), Historical surface faulting in the Basin and Range province, western North America: Implications for fault segmentation, *J. Struct. Geol.*, *13*, 123–136.

Dixon, T. H., S. Robaudo, J. Lee, and M. C. Reheis (1995), Constraints on present-day Basin and Range deformation from space geodesy, *Tectonics*, *14*, 755–772, doi:10.1029/95TC00931.

Dixon, T. H., M. Miller, F. Farina, H. Wang, and D. Johnson (2000), Present-day motion of the Sierra Nevada block and some tectonic implications for the Basin and Range province, North America, *Tectonics*, *19*, 1–24, doi:10.1029/1998TC001088.

Dolan, J. F., D. D. Bowman, and C. G. Sammis (2007), Long-range and long-term fault interactions in Southern California, *Geology*, *35*, 855, doi:10.1130/G23789A.1.

Foy, T. A., K. L. Frankel, Z. M. Lifton, C. W. Johnson, and M. W. Caffee (2012), Distributed extensional deformation in a zone of right-lateral shear: Implications for geodetic versus geologic rates of deformation in the eastern California shear zone-Walker Lane, *Tectonics*, *31*, TC4008, doi:10.1029/2011TC002930.

Frankel, K. L., J. F. Dolan, R. C. Finkel, L. A. Owen, and J. S. Hoeft (2007a), Spatial variations in slip rate along the Death Valley-Fish Lake Valley fault system determined from LiDAR topographic data and cosmogenic ^{10}Be geochronology, *Geophys. Res. Lett.*, *34*, L18303, doi:10.1029/2007GL030549.

Frankel, K. L., et al. (2007b), Cosmogenic ^{10}Be and ^{36}Cl geochronology of offset alluvial fans along the northern Death Valley fault zone: Implications for transient strain in the eastern California shear zone, *J. Geophys. Res.*, *112*, B06407, doi:10.1029/2006JB004350.

Frankel, K. L., J. F. Dolan, L. A. Owen, P. Ganev, and R. C. Finkel (2011), Spatial and temporal constancy of seismic strain release along an evolving segment of the Pacific–North America plate boundary, *Earth Planet. Sci. Lett.*, *304*, 565–576, doi:10.1016/j.epsl.2011.02.034.

Friedrich, A. M., B. P. Wernicke, N. A. Niemi, R. A. Bennett, and J. L. Davis (2003), Comparison of geodetic and geologic data from the Wasatch region, Utah, and implications for the spectral character of Earth deformation at periods of 10 to 10 million years, *J. Geophys. Res.*, *108*(B4), 2199, doi: 10.1029/2001JB000682.

Ganev, P. N., J. F. Dolan, K. L. Frankel, and R. C. Finkel (2010), Rates of extension along the Fish Lake Valley fault and transtensional deformation in the Eastern California shear zone—Walker Lane belt, *Lithosphere*, *2*, 33–49, doi:10.1130/L51.1.

Global Multi-Resolution Topography (GMRT) dataset (2013), Hosted by Marine Geoscience Data System at Lamont-Doherty Earth Observatory of Columbia University, doi:10.1594/IEDA.0001000. [Available at http://www.marine-geo.org/portals/gmrt/, dataset (accessed on 9/1/2013).]

Gold, R., C. dePolo, R. Briggs, A. Crone, and J. Gosse (2013), Late Quaternary slip-rate variations along the Warm Springs Valley Fault System, Northern Walker Lane, California-Nevada Border, *Bull. Seismol. Soc. Am.*, *103*, 542–558, doi:10.1785/0120120020.

Gosse, J. C., and F. M. Phillips (2001), Terrestrial in situ cosmogenic nuclides: Theory and application, *Quat. Sci. Rev.*, *20*, 1475–1560.

Gourmelen, N., T. H. Dixon, F. Amelung, and G. Schmalzle (2011), Acceleration and evolution of faults: An example from the Hunter Mountain–Panamint Valley fault zone, Eastern California, *Earth Planet. Sci. Lett.*, *301*, 337–344, doi:10.1016/j.epsl.2010.11.016.

Hoeft, J. S. (2010), Temporal variations in slip-rate along the Lone Mountain fault, western Nevada, MS thesis, 102 pp., Atlanta, Georgia Institute of Technology.

Hoeft, J. S., and K. L. Frankel (2010), Temporal variations in extension rate on the Lone Mountain fault and strain distribution in the eastern California shear zone-Walker Lane, *Geosphere*, *6*, 917–936, doi:10.1130/GES00603.S2.

Hoeft, J. S., and K. L. Frankel (2012), Preliminary surficial geologic map along the northwest Lone Mountain and Weepah Hills piedmonts, Esmeralda county, Nevada, Nevada Bureau of Mines and Geology Open File Report, Reno, Nev.

Jackson, J., and D. McKenzie (1983), The geometrical evolution of normal fault systems, *J. Struct. Geol.*, *5*(5), 471–482.

Kirby, E., D. W. Burbank, M. Reheis, and F. Phillips (2006), Temporal variations in slip rate of the White Mountain Fault Zone, Eastern California, *Earth Planet. Sci. Lett.*, *248*, 168–185, doi:10.1016/j.epsl.2006.05.026.

Kirby, E., S. Anandakrishnan, F. Phillips, and S. Marrero (2008), Late Pleistocene slip rate along the Owens Valley fault, eastern California, *Geophys. Res. Lett.*, *35*, L01304, doi:10.1029/2007GL031970..

Koehler, R. D., and S. G. Wesnousky (2011), Late Pleistocene regional extension rate derived from earthquake geology of late Quaternary faults across the Great Basin, Nevada, between 38.5°N and 40°N latitude, *Geol. Soc. Am. Bull.*, *123*(3-4), 631–650.

Kohl, C. P., and K. Nishiizumi (1992), Chemical isolation of quartz for measurement of in situ-produced cosmogenic nuclides, *Geochim. Cosmochim. Acta*, *56*, 3583–3587, doi:10.1016/0016-7037(92)90401-4.

Lal, D. (1991), Cosmic ray labeling of erosion surfaces: In situ nuclide production rates and erosion models, *Earth Planet. Sci. Lett.*, *104*, 424–439.

Le, K., J. Lee, L. A. Owen, and R. Finkel (2007), Late Quaternary slip rates along the Sierra Nevada frontal fault zone, California: Slip partitioning across the western margin of the Eastern California Shear Zone-Basin and Range Province, *Geol. Soc. Am. Bull.*, *119*, 240–256, doi:10.1130/B25960.1.

Lee, J., C. M. Rubin, and A. Calvert (2001), Quaternary faulting history along the Deep Springs fault, California, *Geol. Soc. Am. Bull.*, *113*, 855–869.

Lee, J., D. F. Stockli, L. A. Owen, R. C. Finkel, and R. Kislitsyn (2009a), Exhumation of the Inyo Mountains, California: Implications for the timing of extension along the western boundary of the Basin and Range Province and distribution of dextral fault slip rates across the eastern California shear zone, *Tectonics*, *28*, TC1001, doi:10.1029/2008TC002295.

Lee, J., J. Garwood, D. F. Stockli, and J. Gosse (2009b), Quaternary faulting in Queen Valley, California-Nevada: Implications for kinematics of fault-slip transfer in the eastern California shear zone-Walker Lane belt, *Geol. Soc. Am. Bull.*, *121*, 599–614, doi:10.1130/B26352.1.

Lienkaemper, J. J., S. K. Pezzopane, M. M. Clark, and M. J. Rymer (1987), Fault fractures formed in association with the 1986 Chalfant Valley, California, earthquake sequence, preliminary report, *Bull. Seismol. Soc. Am*, *77*, 297–305.

Lifton, Z. M., A. V. Newman, K. L. Frankel, C. W. Johnson, and T. H. Dixon (2013), Insights into distributed plate rates across the Walker Lane from GPS Geodesy, *Geophys. Res. Lett.*, *40*, 4620–4624, doi:10.1002/grl.50804.

McGuire, M., K. M. Keranen, D. F. Stockli, J. D. Feldman, and G. R. Keller (2011), Geophysical characterization of transtensional fault systems in the Eastern California Shear Zone-Walker Lane Belt, Abstract T11A-2275 presented at 2011 Fall Meeting, AGU, San Francisco, Calif., 5–9 Dec.

Nagorsen-Rinke, S., J. Lee, and A. Calvert (2013), Pliocene sinistral slip across the Adobe Hills, eastern California–western Nevada: Kinematics of fault slip transfer across the Mina deflection, *Geosphere*, *9*, 37–53, doi:10.1130/GES00825.S3.

Nishiizumi, K., M. Imamura, M. W. Caffee, J. R. Southon, R. C. Finkel, and J. McAninch (2007), Absolute calibration of ^{10}Be AMS standards, *Nucl. Instrum. Methods Phys. Res., Sect. B*, *258*, 403–413, doi:10.1016/j.nimb.2007.01.297.

Oldow, J. S., G. Kohler, and R. A. Donelick (1994), Late Cenozoic extensional transfer in the Walker Lane strike-slip belt, Nevada, *Geology*, *22*, 637, doi:10.1130/0091-7613(1994)022<0637:LCETIT>2.3.CO;2.

Oldow, J. S., J. W. Geissman, and D. F. Stockli (2008), Evolution and strain reorganization within Late Neogene structural stepovers linking the Central Walker Lane and Northern Eastern California Shear Zone, Western Great Basin, *Int. Geol. Rev.*, *50*, 270–290, doi:10.2747/0020-6814.50.3.270.

Oldow, J. S., E. A. Elias, L. Ferranti, W. C. McClelland, and W. C. McIntosh (2009), Late Miocene to Pliocene synextensional deposition in fault-bounded basins within the upper plate of the western Silver Peak–Lone Mountain extensional complex, west-central Nevada: Late Cenozoic structure and evolution of the Great Basin–Sierra Nevada transition, *Geol. Soc. Am. Spec. Pap.*, *447*, 275–312, doi:10.1130/2009.2447(14).

Olive, J.-A., and M. D. Behn (2014), Rapid rotation of normal faults due to flexural stresses: An explanation for the global distribution of normal fault dips, *J. Geophys. Res. Solid Earth*, *119*, 3722–3739, doi:10.1002/2013JB010512.

Owen, L. A., R. C. Finkel, M. W. Caffee, and L. Gualtieri (2002), Timing of multiple late Quaternary glaciations in the Hunza Valley, Karakoram Mountains, northern Pakistan: Defined by cosmogenic radionuclide dating of moraines, *Geol. Soc. Am. Bull.*, *114*, 593–604.

Owen, L. A., R. C. Finkel, P. L. Barnard, M. Haizhou, K. Asahi, M. W. Caffee, and E. Derbyshire (2005), Climatic and topographic controls on the style and timing of Late Quaternary glaciation throughout Tibet and the Himalaya defined by ^{10}Be cosmogenic radionuclide surface exposure dating, *Quaternary Sci. Rev.*, *24*, 1391–1411, doi:10.1016/j.quascirev.2004.10.014.

Phillips, F. M., and L. Majkowski (2011), The role of low-angle normal faulting in active tectonics of the northern Owens Valley, California, *Lithosphere*, *3*, 22–36, doi:10.1130/L73.1.

Reheis, M. C., and T. H. Dixon (1996), Kinematics of the Eastern California shear zone: Evidence for slip transfer from Owens and Saline Valley fault zones to Fish Lake Valley fault zone, *Geology*, *24*, 339.

Reheis, M. C., and T. L. Sawyer (1997), Late Cenozoic history and slip rates of the Fish Lake Valley, Emigrant Peak, and Deep Springs fault zones, Nevada and California, *Geol. Soc. Am. Bull.*, *109*, 280–299, doi:10.1130/0016-7606(1997)109<0280:LCHASR>2.3.CO;2.

Reheis, M. C., T. L. Sawyer, J. L. Slate, and A. R. Gillispie (1993), Geologic map of late Cenozoic deposits and faults in the southern part of the Davis Mountain 15′ quadrangle, Esmeralda County, Nevada, *U.S. Geol. Surv. Map I-2342*, scale 1:24,000.

Ryan, W. B. F., et al. (2009), Global Multi-Resolution Topography (GMRT) synthesis data set, *Geochem. Geophys. Geosyst.*, *10*, Q03014, doi:10.1029/2008GC002332.

Stone, J. O. (2000), Air pressure and cosmogenic isotope production, *J. Geophys. Res.*, *105*(B10), 23,753–23,759, doi:10.1029/2000JB900181.

U.S. Geological Survey, California Geological Survey (CGS), and Nevada Bureau of Mines and Geology (NBMG) (2006), Quaternary fault and fold database for the United States. [Available at http://earthquakes.usgs.gov/regional/qfaults/, (Accessed on 9/1/2013).]

Weldon, R., K. Scharer, T. Fumal, and G. Biasi (2004), Wrightwood and the earthquake cycle: What a long recurrence record tells us about how faults work, *GSA Today*, *14*, 4, doi:10.1130/1052-5173(2004)014<4:WATECW>2.0.CO;2.

Wells, D. L., and K. J. Coppersmith (1994), New empirical relationships among magnitude, rupture length, rupture width, rupture area, and surface displacement, *Bull. Seismol. Soc. Am.*, *84*, 974–1002.

Wernicke, B. (1981), Low-angle normal faults in the Basin and Range Province: Nappe tectonics in an extending orogen, *Nature*, *291*, 645–648, doi:10.1038/291645a0.

Wernicke, B. (1995), Low-angle normal faults and seismicity: A review, *J. Geophys. Res.*, *100*(B10), 20,159–20,174, doi:10.1029/95JB01911.

Wernicke, B., and G. J. Axen (1988), On the role of isostasy in the evolution of normal fault systems, *Geology*, *16*, 848–851.

Wesnousky, S. G. (2005), Active faulting in the Walker Lane, *Tectonics*, *24*, TC3009, doi:10.1029/2004TC001645.

Wesnousky, S. G., J. M. Bormann, C. Kreemer, W. C. Hammond, and J. N. Brune (2012), Neotectonics, geodesy, and seismic hazard in the Northern Walker Lane of Western North America: Thirty kilometers of crustal shear and no strike-slip?, *Earth Planet. Sci. Lett.*, *329*, 133–140.

Zechar, J. D., and K. L. Frankel (2009), Incorporating and reporting uncertainties in fault slip rates, *J. Geophys. Res.*, *114*, B12407, doi:10.1029/2009JB006325.

Zehfuss, P. H., P. R. Bierman, A. R. Gillespie, R. M. Burke, and M. W. Caffee (2001), Slip rates on the Fish Springs fault, Owens Valley, California, deduced from cosmogenic ^{10}Be and ^{26}Al and soil development on fan surfaces, *Geol. Soc. Am. Bull.*, *113*, 241–255, doi:10.1130/0016-7606(2001)113<0241:SROTFS>2.0.CO;2.